Available online at www.sciencedirect.com

ScienceDirect

Procedia Engineering 103 (2015) 663 – 670

Procedia Engineering

www.elsevier.com/locate/procedia

The 13th Hypervelocity Impact Symposium

Shaped Charge Jet Penetration of Alon® Ceramic Assessed by Proton Radiography and Computational Simulations

Michael B. Zellner[a*], Richard Becker[b], Dattatraya P. Dandekar[c], Richard B. Leavy[d], Parimal J. Patel[e] and PRad Team[f]

[a]*U.S. Army Research Laboratory, Attn: RDRL-WMP-D, Aberdeen Proving Ground, MD 21005, michael.b.zellner.civ@mail.mil*

[b]*U.S. Army Research Laboratory, Attn: RDRL-WMP-C, Aberdeen Proving Ground, MD 21005, richard.c.becker.civ@mail.mil*

[c]*U.S. Army Research Laboratory, Attn: RDRL-WMP-C, Aberdeen Proving Ground, MD 21005, dattatraya.p.dandekar.ctr@mail.mil*

[d]*U.S. Army Research Laboratory, Attn: RDRL-WMP-C, Aberdeen Proving Ground, MD 21005, richare.b.leavy.civ@mail.mil*

[e]*U.S. Army Research Laboratory, Attn: RDRL-WMM-E, Aberdeen Proving Ground, MD 21005, parimal.j.patel.civ@mail.mil*

[f]*Los Alamos National Laboratory, MS-H803, Los Alamos, NM 21545, asaunders@lanl.gov*

Abstract

This work describes the use of proton radiography and continuum simulations to investigate the mechanics of a copper jet penetrating unconfined ALON® transparent ceramic. Use of proton radiography enabled characterization of the jet and ceramic material at 21 time steps, *in situ,* throughout the penetration process. These radiographs provide time-evolution data pertaining to the material densities, cavity growth, and material failure. The data were compared to legacy analytical penetration models and to a simulation of the event computed using a continuum multi-physics code. These comparisons revealed additional insights into the penetration mechanics as well as strengths and weaknesses of the computational algorithms and material models used in the simulations.

Peer-review under responsibility of the Curators of the University of Missouri On behalf of the Missouri University of Science and Technology

Keywords: Ceramic, ALON, Shaped charge jet, Kayenta, ALEGRA, continuum simulation, Proton Radiography

1. Introduction

The response of ceramics to static and dynamic compression/unloading cycles is often unique from those in other classes of materials. A few distinctive material properties that contribute to these responses are: relatively high elastic moduli, fast wave propagation speeds (> 10 km/s), fracture toughness near a few MPa*m$^{1/2}$, high compressive strengths, low tensile strengths, and they typically fail in a brittle manner. Since many of these responses deviate significantly from other materials, inclusion of ceramics in studies of problems undergoing static and dynamic compression/unloading cycles is useful.

Empirically, unconfined bulk ceramics have been found to impart minimal influence, beyond hydrodynamic erosion, on high-speed penetrating jets when compared to other classes of materials such as metals and glasses [1-6]. Even polymers, when compared on a per mass basis, have substantially higher effectiveness at influencing jets than ceramics. The predominate interactions effecting high-speed penetrating jets include mechanisms such as erosion and foreshortening [7], and impartment of off-axis momentum through more complex jet/material interactions that are related to the elastic/plastic and failure/particulation response of the materials involved. Because empirical results demonstrate that jets are minimally influenced by ceramics, it is hypothesized that the interaction mechanisms are modified by the extreme properties/responses

* Michael B. Zellner. Tel.: 410-306-2565 ; Fax.: 410-278-6061

Email address: michael.b.zellner.civ@mail.mil

Peer-review under responsibility of the Curators of the University of Missouri On behalf of the Missouri University of Science and Technology

doi:10.1016/j.proeng.2015.04.086

of ceramic materials. This hypothesis can be tested by conducting a high fidelity experiment of a jet penetrating ceramic material, focused on observing the material response *in situ* and inferring how its properties contributes to the known (and possibly novel) mechanisms influencing the jet.

In this work we assess, both computationally and experimentally, the hypervelocity penetration of a copper jet through unconfined ALON® ($Al_{23}O_{27}N_5$) optical ceramic [8] to determine the effect of the aforementioned material properties on penetration mechanics. More specifically, this work combines continuum simulations and *in situ* proton radiographic [9,10] measurements of the compression, subsequent release states, and fracture, in a high-pressure, dynamic environment created around a high-speed copper jet penetrating two stacked ALON® disks. ALON® was chosen specifically because it is a transparent ceramic, which will allow for future measurements of fracture/failure using optical based techniques. The test setup is also such that for these future experiments, the loading will be applied interior to the sample, so many of the complications due to surface-initiated fracture obscuring the bulk response are ameliorated.

Of particular importance in the current study is the use of an experimental technique capable of collecting numerous radiographs in real time during a single penetration event. The experimental measurements of the dynamic fracture and compression were made using 800 MeV proton radiography at the Los Alamos Neutron Science Center facility of Los Alamos National Laboratory (LANL), to assess material density and flow [11]. This time-evolution data also allowed for direct verification and validation of theoretical models.

The computational portion of this study was performed using an arbitrary Lagrangian-Eulerian continuum finite element code ALEGRA, developed by Sandia National Laboratory [12]. The ceramic material was characterized by the Kayenta constitutive model. The simulations were run using an improved XFEM interface tracking method [13].

2. Experimental Methods

To assess the material interactions, proton radiography imaged, *in situ*, a metallic jet penetrating two stacked ALON disks along their symmetry axis. A schematic of the experimental setup is displayed in Figure 1. The disks of diameter d = 50.8 mm and length l = 25.4 mm were stacked together without binder. The raw material was purchased and machined from Surmet [8] and some of its material properties are listed in Table 1. With the current experimental configuration and the materials probed, LANL's proton radiography facility has the capability to resolve absolute density with a 3-4% error [11].

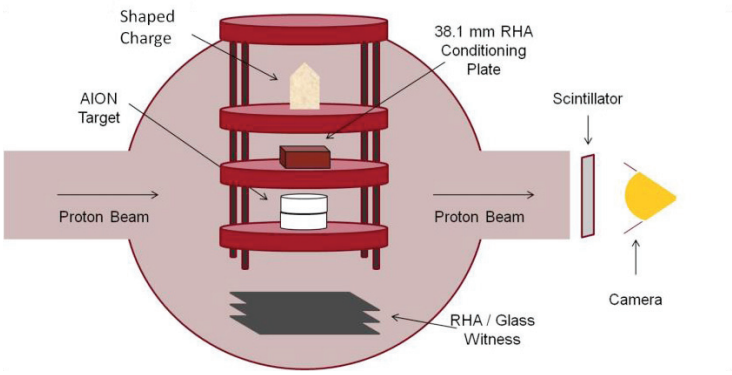

Figure 1. Experimental setup used to collect proton radiography data.

Table 1. Physical properties of ALON® listed by manufacturer (Surmet).

Property	Value
Density	3.69 g/cm^3
Grain Size (typical)	200 – 300 µm
Melting Temperature	2150 C
Young's Modulus	320 GPa
Shear Modulus	135 GPa
Poisson Ratio	0.24
Hardness	1800 Kg/mm^2 (Knoop Indentation, 200g load)
Fracture Toughness	2.0 MPa-m$^{1/2}$
Thermal Conductivity	12.6 W/mK (@ 25 C)

The jet used to penetrate the ALON targets was formed by a shaped charge of approximately 0.5 Kg of LX-14 high explosive collapsing a 65 mm diameter copper cone. Detonation of the shaped charge in vacuum forms a jet with a 9.25

mm/μs non-stretching tip particle (l ~ 18 mm, d ~ 6 mm) which is followed by a stretching cylindrical jet (approximately 3 – 4 mm in diameter). A detailed analysis of the jet and its formation in air was performed by Zellner and Vunni [14] and some characteristics of the jet were measured by Summers [15]. For the current study, it was desired to have a jet without a large tip particle and of a maximum velocity appreciably lower than the wave speed of the target material. To establish these impactor conditions, the jet was conditioned by penetrating a 38.1 mm thick steel plate offset 50.8 mm from the shape charge liner base. Penetration within this plate erodes the early portion of the jet, leaving only the portion of the jet traveling slower than approximately 7 mm/μs, which continues on with slight foreshortening effects to penetrate the ALON targets. One small nuance of conditioning a jet in this manner is the formation of spall off of the rear surface of the conditioning plate, which also impacts the targets, albeit at a slightly later time than the jet tip.

During the experiment, the target and shape charge were suspended near the center a 2 m diameter high explosive containment vessel at the LANL proton radiography facility. This vessel was sealed and a vacuum of approximately 200 torr was established prior to detonation of the high explosive. The shaped charge and target materials were supported by plastic plates that were suspended from threaded rod attached to the top of the vessel. The configuration was oriented to shoot in a top-down orientation (along with gravity), and it used a 130 mm standoff between the shaped charge and the impact surface of the target. To minimize boundary effects, the plastic target support plate was drilled creating a 44.45 mm diameter hole so that the target material was only supported by the outer 3.125 mm of its radius. Additionally, a small amount of epoxy was used to affix the target to the support.

Generally, the radiographic images were capable of imaging a 110 mm x 110 mm field of view using a 1x quadrapole electromagnetic magnification lens configuration. The radiographs were captured by scintillating approximately 60 ns duration bunches of protons using a Lu0 6Y1 4Si0 5:Ce (LYSO) scintillator and numerous cameras. The scintillator had a decay half-life of approximately 40 ns, which was paired with a 80 ns camera gate time to collect the images. The resulting images had approximately 200 μm spatial resolution, and approximately 60 ns temporal resolution (blurring).

3. Simulation Methods

Simulations of the jet, target, conditioning plate and support materials were computed using ALEGRA continuum multi-physics code [12] run on the U.S. Army Research Laboratory's high performance computing system. The simulations shown utilized the extended finite element (XFEM) capabilities along with Lagrangian material tracking in ALEGRA. These methods are under development and were employed to mitigate advection issues with damage and better resolve material interfaces. A snapshot of the simulation depicting the computational space just prior to jet interaction with the conditioning plate is shown in Figure 2. The simulation was computed using two-dimensional, cylindrical symmetry. Formation and conditioning of the jet employed Mie-Gruneisen equations-of-state for the copper and steel components, paired with Steinberg-Guinan constitutive models and Johnson-Cook fracture criteria. The plastic support structures used a Mie-Gruneisen equation-of-state, with elastic/perfectly-plastic constitutive equations. A robust discard statement was necessary to avoid superheating of very small particles ejected from the copper/steel conditioning interaction. Detonation of the shaped charge utilized a Jones-Wilkson-Lee equation of state, paired with a programmed burn to control the reaction front.

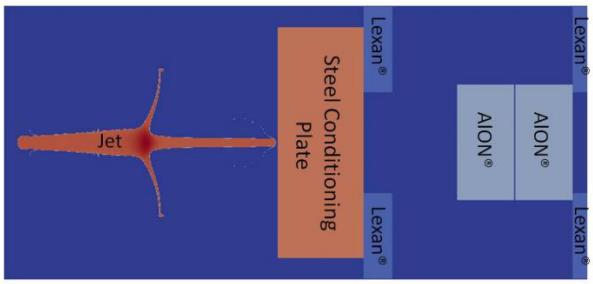

Figure 2: Image of computational layout just prior to the jet impacting the steel conditioning plate.

The target material was modeled using a Mie-Gruneisen equation of state with Kayenta constitutive model [16-18] parameterized for aluminum oxynitride. Kayenta is a generalized plasticity model used to describe ceramics at the macroscopic continuum level. The limit surface of a material element essentially describes the three-dimensional stress state-dependent mechanical response of that element. Kayenta allows for third invariant dependence, softening, hardening,

and porosity. A Weibull distribution describes variability of material strength in hydrostatic tension. This variability is scaled based on the local finite element size, with a time-to-failure criterion restricting damage to propagate at the same speed regardless of element size. This model was parameterized to the following: a crack velocity equal to 10% of the longitudinal wave speed (1.037 mm/μs); a Weibull coefficient of 23.7; and a 233 μm aggregate size (grain size) used to characterize the variability. The Kayenta limit surface was calculated using an ancillary mesoscale model [19], which demonstrated realistic performance.

4. Results and Discussion

Prior to the jet impacting the target, four radiographs were acquired to characterize the jet and spall cloud profiles. Erosion of the jet during the conditioning plate interaction resulted in a jet tip velocity of 7.1 ± 0.5 mm/μs as determined from the radiographs. Figure 3 shows a series of eight radiograph snapshots taken just prior to (the upper leftmost panel) and throughout the penetration event. This is only a portion of the 21 radiographs acquired throughout the experiment. The time-stamp applied to each image is referenced to jet touchdown on the target surface. With exemption of the first image, which was acquired to visualize the jet and spall debris cloud from the steel conditioning plate prior to impact, the frames displayed were acquired 2.25 μs apart. For visualization, the radiographs were divided by a static radiograph acquired just prior to the dynamic experiment, and the contrast was adjusted to accentuate density and cavity features. This process effectively normalizes the images with respect to specimen thickness so that density gradients and the penetration cavity are more readily discerned.

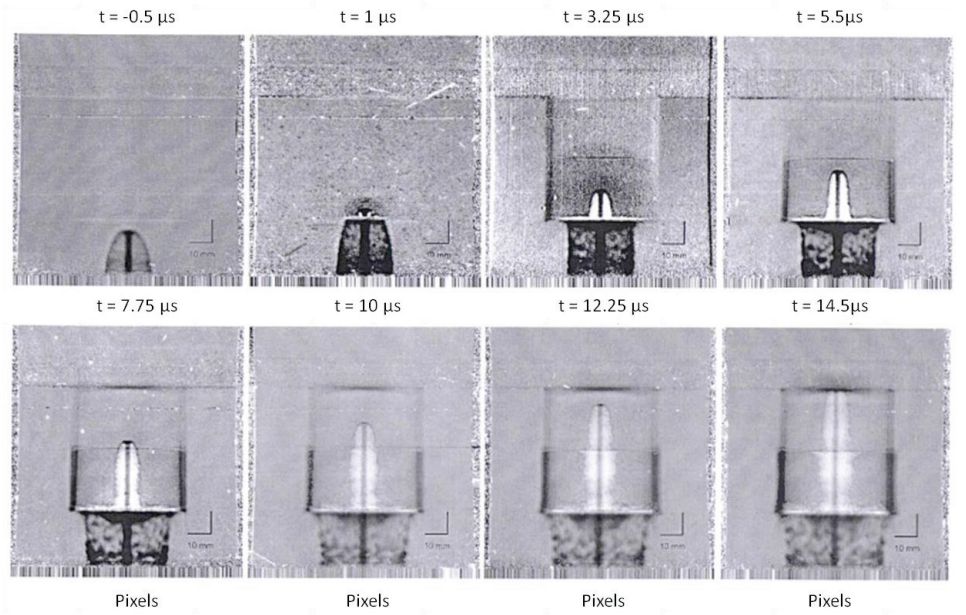

Figure 3: Eight proton radiograph snapshots of a copper jet penetrating two ALON discs.

Upon impact, the jet's momentum compresses the target material. Because of the configuration symmetry and the sound speed in ALON, a dispersive compression front expands spherically from the initial impact. In Figure 3 this is observed in the images acquired 1-, 3.25-, and 5.5-μs after impact as dark halos of lessening intensity (note that because the images were individually contrast adjusted, the apparent intensity deviates from the expected radius-squared fall-off). The position of the expanding compression front as a function of time is plotted in Figure 4. From this plot, a longitudinal sound speed of 10.53 ± 0.1 mm/μs is measured for the ALON material. This is slightly higher than the 10.11 mm/μs calculated when assuming an isotropic, homogeneous material and using the manufacturer's quoted density, Young's modulus, and Poisson ratio [8].

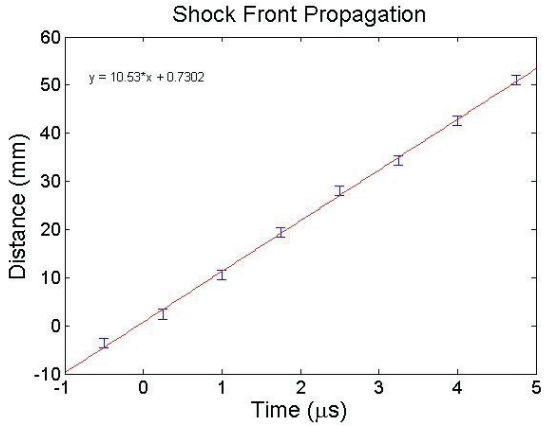

Figure 4: Compression front position extracted from the radiographs.

Following expansion of the compression front, the jet penetrates the material forming a hollow cavity. Figure 5 plots the jet tip position as a function of time during the penetration process. Overlaid on this plot are four vertical dashed lines that temporally correspond to: the interaction of the dispersive compression front with the ALON/ALON interface and the ALON target radial boundary; the interaction of the expanding dispersive compression front with the ALON target's rear surface; the time at which the jet interacts with the ALON/ALON interface; and the time at which the jet exits the ALON target. Because of the high fidelity of the penetration measurements, the current data can be compared to predictions from penetration theories, such as hydrodynamic penetration theory [20, 21], which gives the penetration velocity, U, as:

$$U = V\left(1 + \left(\rho_t/\rho_j\right)^{1/2}\right)^{-1} \tag{1}$$

In Equation 1, V is the impact velocity, ρ_t is the target density, and ρ_j is the jet density. In its presented form, Equation 1 is valid for steady state penetration of a rod of constant velocity. The impacting jet has an approximately linear velocity gradient along its length, and the tail of the jet has a velocity near 2.0 mm/μs. Hydrodynamic calculations using formation theory, and correcting for erosion and foreshortening, predict that 2-3 mm of the jet will be eroded upon exit of the 50.8 mm thick ALON target and that the jet velocity will be approximately 6.3 mm/μs upon exit. Substituting the impact velocity of 7.1 mm/μs, and the exit velocity of 6.3 mm/μs into Equation 1 predicts the penetration velocity will decay from 4.3- to 3.8-mm/μs through the target. Plots for these two calculated penetration velocities are overlaid on Figure 5 for comparison. The slopes of the data at the entry and exit are consistent with the corresponding lines, with a relatively smooth transition in between, indicating that the copper jet propagation through ALON is consistent with hydrodynamic penetration theory.

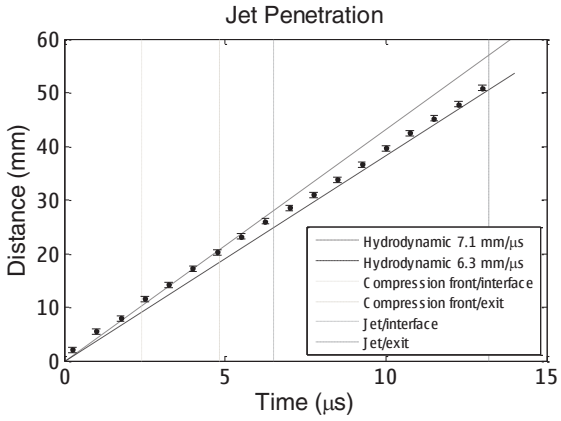

Figure 5: Jet tip position extracted from the radiographs during target penetration.

Applicability of the hydrodynamic penetration model to ceramic jet penetration is important because it reveals that strength effects within ALON are insignificant even though ALON's hardness is an order of magnitude greater than steels (steel Knoop Hardness ~250 Kg/mm^2)[8]. A hypothesis of the penetration mechanism can be made in which fracture propagates ahead of the jet penetration, creating a scenario in which the jet is penetrating small comminuted particles of ALON ceramic. In this case, if the particles have a radius much less than the radius of the jet, bulk material strength would not play a role and granular flow mechanisms would be operative. This scenario is plausible when considering that the fracture toughness is an order of magnitude less for ceramics than steels (~50 MPa-m$^{1/2}$), and that the fracture front speed has been measured near 9.8 mm/μs for lower velocity ballistic impacts [22, 23].

Because the radiographs have approximately 200 μm spatial resolution, they provide information about some gross fracture/failure phenomena and development of the penetration channel. These observations can be compared to computational results of the coherence parameter, which reflects the evolution of the material limit surface as damage progresses. Figure 6 shows damage (coherence or "COHER" of 0 = fully damaged, "COHER" of 1 = fully intact material) mapped at multiple time-steps throughout the penetration process to compare with the radiographs of Figure 3. Experimentally, the jet opens an approximately 10 mm diameter cavity in the ALON target immediately following impact. The calculated cavity size is consistent with this measurement. The experimental cavity is characterized by relatively smooth sidewalls, along which jet erosion products collect (indicated by large proton attenuation). The copper accumulated along the cavity walls is evident in Figure 3. The radiographs also show significant deformation of the impacted surface and contrast variations near the target surface at larger radial distances that result from accumulation of steel debris ejected during jet penetration of the conditioning plate. Simulations suggest that these impacts initiate a significant amount of failure in the target material. The simulations show damage from the debris impact at large radial distances initiating fracture and surface deformation.

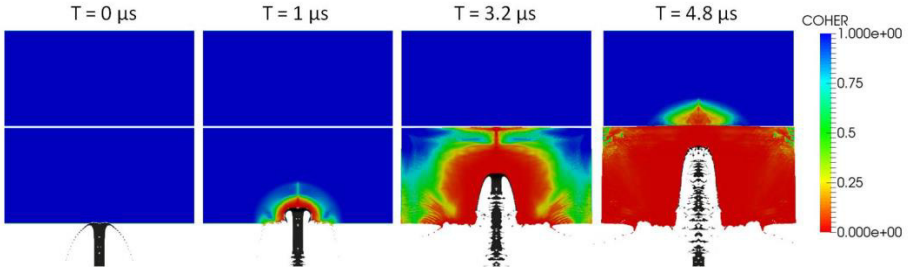

Figure 6: Computed coherence as a jet penetrates two cylinders of ALON®.

Simple calculations using the experimentally measured fracture propagation velocity suggest that by 2.6-3.6 μs after impact, forward propagating fracture from the impact point should permeate throughout the entire first target cylinder. The continuum simulations tend to agree with this estimate, although a precise interpretation of target coherence variable with regards to fracture is a vague, and radial fracture cannot be represented in an axisymmetric simulation. It is evident from Figure 6, however, that the entire first cylinder has failed by 4.8 μs. To substantiate claims of complete first cylinder failure, the radiograph imaged 5.5 μs after impact is particularly interesting. Recall that the radiographs displayed have been divided by a static image. In this analysis methodology, contrast relates to material change or movement. In this image, the jet has not yet reached the ALON/ALON interface, but the entire first cylinder has a much darker contrast than the second cylinder. This supports the hypothesis that fracture permeated throughout the first cylinder. In addition, a small volume at the outer radius of the first cylinder has very high contrast in this normalized image, which is consistent with expansion of the first disk.

The lack of contrast change in the second cylinder supports a hypothesis that fracture propagation is inhibited by the interface. This phenomenon is also observed in the simulations, which used the XFEM routine to represent material interfaces. The simulations do, however, display reduced coherence values in the second cylinder of ALON prior to the jet penetrating this layer. This observation must result from fracture during transmission of the dispersive compression front, as the shear stress is not transmitted across the interface.

After approximately 7 μs, some features of lesser proton attenuation, interpreted as possible separation of material and formation of large scale radial cracks, can be seen near the impact surface and at larger radial distances within the target. During this time, the initial outward propagating compression wave should have reached and reflected from the target's radial boundary. It in unknown how much of the material enters a tensile state from this reflected wave, as forward

propagating fracture inhibits the material's ability to communicate the reflected tensile mechanical waves. Discrete radial cracks cannot be represented in the axisymmetric simulations.

After approximately 10 μs, the penetration cavity shape begins to distort significantly. The distortion appears to be linked to delayed failure transmission and slip across the ALON/ALON interface. Very near the interface, the penetration cavity begins to widen, forming a conical section with broadening "wings" expanding near the interface. The second ALON cylinder, however, does not display any broadening, forming a discontinuous step of material inside the penetration cavity as it spans the material interface. Within the first ALON cylinder, the conical broadening at the interface is accompanied by less broadening of the entry portion of the penetration channel, with the cavity a few mm from the impact point showing little continued expansion. This may be related to stress relief near the interface, or possibly even from material flow associated with the impact of the conditioning plate debris. Unfortunately, the enhanced simulations with XFEM fail prior to capturing these interactions and the modeling provides no insight into the mechanism.

One noticeable effect of the overall penetration experiment is that, outside of the material in the immediate vicinity of the impact, the apparent material density continues to decrease relatively uniformly throughout the experiment's duration. In other materials such as polymers, the momentum transfer leads to significant extended compression and in some cases irreversible phase changes within target material. The continual decrease of the apparent material density is presumed to be linked to the brittle nature of ALON paired with its quick fracture propagation, resulting in constant radial expansion of the fractured material. It is also noted that confinement of the particles would likely alter the penetration dynamics significantly. Continuum simulations appear to produce similar decreasing density results.

5. Summary

In this work, we have presented a proton radiography characterization of ALON's material response, *in situ* during penetration by a copper jet. The high spatial and temporal fidelity of the technique allowed for an accurate mapping of the compression front, the jet penetration, and penetration cavity development. It was found that impact of a jet traveling 7.1 mm/μs forms a dispersive compression front that propagates throughout the target material at a velocity of 10.53 ± 0.1 mm/μs. The radiographic evolution detailed that after the initial impact, the jet forms an approximately 10 mm diameter penetration cavity, through which the remaining portions of the jet traverse relatively uninterrupted. The penetration of the jet through the target was found to agree with hydrodynamic theory, implying that the high hardness of the ceramic target did not contribute significantly to the penetration dynamics. It was hypothesized that any effect of hardness was negated because fracture permeated the sample at a velocity greater than the penetration velocity. Proton radiography also provided information on the materials fracture/failure response. The radiographs imply that fracture in the second cylinder of ALON was delayed due to lack of transmission of fracture and shear stress across the ALON/ALON interface. The cavity near the interface also demonstrated unique "late time" features, hypothesized to originate from the discontinuous mechanical response across the interface.

Coherence plots (inverse of failure) from the simulations generally agreed with the inferred fracture/failure response extracted from the experiments. The simulations were capable of predicting discontinuous failure propagation across the ALON/ALON interface, but did show fracture nucleation across the interface as the penetrator neared the second disk. The simulations, however, are a bit vague in the correspondence of coherence value with failed material, allowing for subjective interpretation. Similarly, the density decrease associated with fracture may be below the resolution of the experiments, leading to subjective interpretation of fracture. The simulations were also capable of reproducing the reduced apparent target density observed in the experiments. Continued simulations to longer times are needed to make further comparisons to the cavity profile and penetration rates.

Acknowledgements

The authors would like to acknowledge funding for this project through U.S. Army Research Laboratory (ARL) mission funding. We would also like to acknowledge the assistance of personnel at LANL's proton radiography facility, who assisted with the experimental setup. We would also like to thank the Distributed Shared Resources Center, part of the DoD High Performance Computing Modernization Program, located at the Aberdeen Proving Ground for access to the computational resources.

References

[1] WEI Xue-ying , ZHANG Chun-yan, MA Shu-fang, 2005. Resistance and Property of Ceramic Target Against Shaped-charge Jet Penetration Acta Armamentarii

[2] Hornemann, U., Holzwarth, A., 1997. Shaped charge penetration in alumina targets, Int. J. Impact. Eng. 20, p. 375

[3] Eichelberger, R.J., 1956. Experimental Test of the Theory of Penetration by Metallic Jets, J. Appl. Phys. 27, p. 63

[4] Hornemann, U., 1989. "The terminal ballistic resistance of glass against shaped charge penetration," Proc. 11th Int. Symp. Ballistics, Vol. II, pp. 381–389

[5] Hauver, G.E., Netherwood, P.H., Benck, R.F., Melani, A., 1991. Penetration of Shaped-Charge Jets into Glass and Crystalline Quartz: BRL-TR-3273, U.S. Army Ballistics Research Laboratory, 1991.

[6] Moran, B., Glenn, L.A., Kusubov, A., 1991. Jet penetration in glass, J. Phys. IV France 01, p. C3-147

[7] Svirsky, O.V., Kovalev, N.P., Klopov, B.A., Bashurov, V.V., Krutyakov, V.A., 2001. The shaped charge jet interaction with finite thickness targets, Int. J. Impact. Eng. 26, p. 735

[8] Warner, C.T., Hartnett, T.M., Fisher, D., Sunne, W., Characterization of ALON™ Optical Ceramic. In SPIE Proceedings, volume 5786

[9] Golubev, A.A., Demidov, V.S., Demidova, E.V., Dudin, S.V., Kantsyrev, A.V., Kolesnikov, S.A., Mintsev, V.B., Smirnov, G.N., Urtikov, V.I., Utkin, A.V., Fortov, V.E., Sharkov, B.Y., 2010. Diagnostics of fast processes by charged particle beams at TWAC-ITEP accelerator-accumulator facility, Technical Physics Letters 36, p. 177

[10] Merrill, F. and the pRad Collaboration, Proton Radiography Primer; LA-UR-08-07298; Los Alamos National Laboratory, 2008. http://lansce.lanl.gov/pRad/index.shtml.

[11] Morris, C.; Hopson, J. W.; Goldstone, P., 2006. Proton Radiography, Los Alamos Science 30, p. 32

[12] Carroll, S.K., Drake, R.R., Hensinger, D.M., Luchini, C.B., Petney, S.V., Robbins, J., Robinson, A.C., Summers, R.M., Voth, T.E., Weirs, V.G., Wong, M.K., Brunner, T.A., Garasi, C.J., Haill, T.A., Hanshaw, H.L., Mehlhorn, T.A., ALEGRA: SAND2004-6541 , Sandia National Laboratory, January 2005

[13] Moës, N., Dolbow, J., Belytschko, T., 1999. A finite element method for crack growth without remeshing,. International Journal for Numerical Methods in Engineering 46 (1), p. 131

[14] Zellner, M.B., Vunni, G.B., 2013. Photon Doppler Velocimetry (PDV) Characterization of Shaped Charge Jet Formation, Procedia Engineering 58, p. 88

[15] Summers, R. Personal Communication: U.S. Army Research Laboratory, 1996.

[16] Brannon, R., Fossum, A. Strack, E., Kayenta: Theory and User's Guide: SAND2009-2282, Sandia National Laboratories, 2009.

[17] Brannon, R., Strack, E., Leavy, B., Aleatory Uncertainty and Scale Effects in Damage Models for Failure and Fragmentation, Part I: Theory and Calibration, Int J. Fracture, to appear.

[18] Brannon, R., Strack, E., Leavy, B., Aleatory Uncertainty and Scale Effects in Damage Models for Failure andFragmentation, Part II: Verification and Validation, Int J. Fracture, to appear.

[19] Leavy, R.B., Clayton, J.D., Strack, O.E., Brannon, R.M., Strassburger, E., Edge on impact simulations and experiments: In Hyper Velocity Impact Society Symposium Procedings 58, 2013.

[20] Birkhoff, G., Zarantonello, E.H., 1957. Jets, Wakes and Cavities, Academic Press, New York, NY

[21] Caywood, T.E., Birkhoff, G., 1949. Fluid flow patterns. J. Appl. Phys.,

[22] Strassburger, E., Senf, H., Experimental Investigations of Wave and Fracture Phenomena in Impacted Ceramics and Glasses: ARL-CR-214, US Army Research Laboratory, February 1995.

[23] Strassburger, E., High Speed Photographic Study of Wave Propagation and Impact Damage in Transparent Aluminum Oxynitride: ARL-CR-579, US Army Research Laboratory, April 2006.